Comparing a Dynamic Railgun Simulation with Experiment

S. Hundertmark
ISL, French-German Research Institute of Saint-Louis
5 rue du Général Cassagnou, 68301 Saint Louis, France
e-mail: Stephan.Hundertmark@isl.eu

***Abstract*:** *Today progress in railgun research is usually achieved experimentally with support from static simulations. It is of great interest to set up dynamic simulations that allow to asses time dependent information about the parameters involved in the electromagnetic acceleration of masses. In this investigation a dynamic 3-d finite element simulation of a small, 28 mm caliber railgun was implemented. The novelty of this approach is, that after a simulation run, the time history of, for example the velocity of the projectile is available. To validate the simulation results, a series of shots with a 28 mm caliber railgun was performed. Good agreement between the experiment and the dynamic simulation was observed.*

***Key words*:** *Railgun, electromagnetic launcher, inductive gradient, lprime, finite element simulations.*

1. Introduction

Electrical machines are complicated setups, involving the interplay of electrical, magnetic and mechanical effects. In the design and optimization of such machines a multitude of analytic, simulation or combined methods are applied (to name just two examples, see [1], [2]). One type of an electrical device that pushes the limits of the existing technologies is the railgun. An electric railgun is a device that uses the Lorentz force to propel masses to typically large velocities. One of the driver for the development of railguns was and is the military, as can be seen for example in the current development of the largest railgun installation in the world, the US-naval railgun [3]. Nevertheless, the inherent flexibility in masses to be accelerated and in velocity range allow for a multitude of possible applications in the civilian sector. Same of these would be the launch of small satellites [4], the disposal of nuclear waste into the depth of space [5], the injection of pellets into a fusion reactor [6] or as a tool for material research [7], [8]. Apparently, the wide field of applications with very different requirements can not be served with one implementation of the railgun principle, instead there is a large range of technical variations, quite a few being summarized in [9], [10].

Analytic calculations and simulations are being used to design and optimize railguns, but the extreme conditions and the many physical process being involved during the acceleration make an accurate modeling of a firing railgun a difficult task. Therefore the design efforts usually concentrate on the most important key-parameters and use simplified simulations. Recent examples for this approach are [11], analytically optimizing for two parameters, the geometrical inductance gradient and the allowable current density and [12] using 2-d finite element simulations and lumped parameter models to evaluate a large number of different geometries. In [13] the authors implement a static 3-d railgun model, solving the Maxwell equations for an array of fixed projectile velocities.

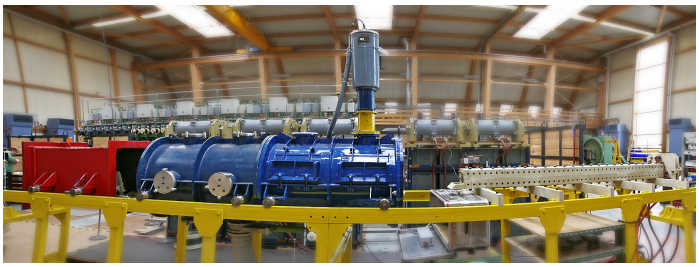

Fig. 1. The small caliber railgun SR\3-60.

At the ISL[1], the railgun group launched an effort to use the modern finite element program COMSOL [14] with the goal to set up a realistic dynamic, moving projectile simulation in 3-d. To the authors knowledge, this is the first time such a simulation is performed and compared to experimental data.

2. Experimental Setup

One of the smaller railguns installed at the ISL is the SR\3-60 [15]. Figure 1 shows the railgun to the right hand side. The SR\3-60 is a segmented railgun with three segments and a total barrel length of 225 cm. Each segment is connected to a 150 kJ capacitor bank (visible in the background of the figure) with a typical pulse length of about 10 ms. Due to its internal configuration, the segments can be used sequential, in parallel or individually. In this investigation the gun is used as simple railgun, using one pair of 75 cm long rails and one capacitor bank. The aluminum box in the center of the picture, just under below the muzzle, houses a Doppler radar. This device allows to accurately determine the velocity of the projectile during the acceleration process. The left hand barrel is used to install further instrumentation to investigate projectile properties during its free flight phase. Finally, the red box to the very left of the picture stops the flight of the projectile. The rail cross-section is shown in figure 2. Each rail is assembled of two copper bars, one with a width of 20 mm and a height of 10 mm, another with 12 mm and 15 mm, respectively. The projectile is made out of glass-fiber reinforced plastic and makes use of a 8 mm diameter, copper wire brush. The caliber of the projectile is 28 mm,

[1]The French-German Research Institute of Saint-Louis, France

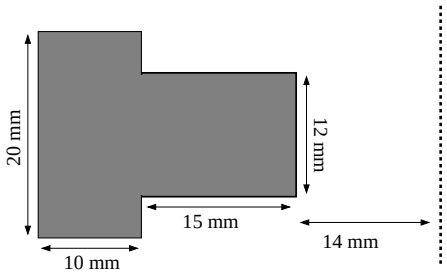

Fig. 2. Cross-sectional view of the rail geometry. Shown is one rail and the distance to the mirror line (on the right hand side).

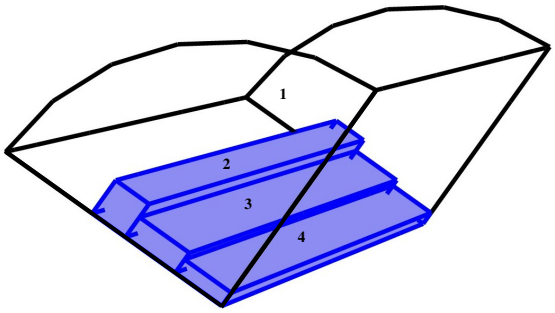

Fig. 4. A 3-d view of the simulation model for the SR\3-60 in COMSOL. Due to symmetries only a quarter of the railgun needs to be modeled. The areas marked by numbers are the following: (1) the surrounding air volume, (2+3) the current carrying rail and (4) the volume in which the brush moves.

with the brush having a small over length to ensure good electrical contact during the acceleration process. The average weight of the used projectiles is about 92 g. The measured current and velocity distribution for a typical shot performed with the SR\3-60 is shown in figure 3. As the inset shows, the doppler radar signal stabilizes only after approximately 0.7 ms, allowing for an accurate determination of the projectile velocity only after this time.

2.1. Dynamic Simulations using a 3-d Model

Implementing a realistic railgun with a moving projectile as a 3-d model in a finite element simulation is a challenge in itself. The size of the mesh is dictated by the physics that influences the acceleration. In this case, the current distribution in the rails is strongly influenced by the skin effect, at higher velocities the velocity skin effect comes into play, too. To correctly model the current distribution therefore requires a mesh size with dimensions smaller than the skin depth. The skin depth is a strong function of the frequency. For the frequencies being involved in a discharge of a capacitor bank, the typical size is of the order of millimeters. This scale is in stark contrast to the longitudinal dimensions of a railgun, which is of the order meter(s). An even more severe complication is that the full simulation of a moving

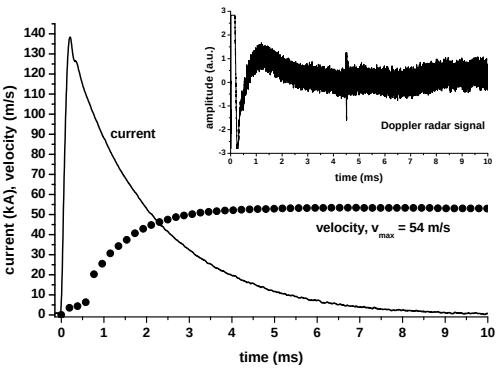

Fig. 3. The current and velocity distribution for a typical SR\3-60 shot. The signal from the doppler radar is shown as inset in the upper left corner.

projectile requires a stationary and a moving mesh. Even so COMSOL is capable of simulating moving meshes, the railgun simulation was simplified by following the example in [19]. There the armature is represented by a volume of material with the conductivity of the corresponding metal, being surrounded by an insulator. To simulate the movement, the position of the armature is recalculated for each time step. This position is used to change the conductivity of the corresponding volume of the space in between the rails. This procedure involves no movement of the mesh. By attaching the weight of the projectile to this region, and using the value of the Lorentz force derived for every time step by the simulation, the acceleration of the projectile is calculated. From the acceleration and the known size of the time step in the simulation, the velocity and position of the projectile is derived. This value is then used in the next time step. The geometrical setup is shown in figure 4. Using the usual symmetries for the simple railgun implementation in 3-d FEM modeling, only a quarter of the problem is simulated. The cylindrical volume around the railgun (marked by (1) in the figure) is filled by air, the current carrying rail is the above mentioned composite of two sections marked with (2) and (3). Within the region (4) the conductivity of the mesh elements is changed at the current position of the armature in a volume corresponding to the volume the armature. The current pulse being driven through the railgun is a smoothed, measured pulse as shown in figure 3. To compare the simulation to experiments being performed with different primary energies, the pulse height (maximum current) was adjusted accordingly. During a simulation run, the so simulated armature will travel in this volume from left to right. A more detailed description of the implementation can be found in [20].

1) Simulation Results: The well known railgun force law can be written as (direction of flight along the z-axis):

$$F_z(t) = m \cdot a(t) = \frac{1}{2} L' I(t)^2. \qquad (1)$$

The velocity of the projectile is gained by integrating equation 1 over the acceleration time (from $t = 0$ to $t = t_f$). The right hand side of equation 1 implies that L' is a constant, being fixed by the geometry of the accelerator. But, due to

the development of the driving current pulse and the magnetic field in the vicinity of the armature, the inductance gradient L' is becoming a function of time. Further on, the current running through the armature will interact not only with the magnetic field behind the center of the armature, but will also "see" the magnetic field in front of it. Thus the inductance gradient being relevant for an dynamic experiment will be reduced compared to the calculated geometrical inductance gradient value. In the above formula these effects can be taken into account by replacing the inductance gradient L' with an averaged, constant, so called effective inductance gradient, L'_{eff} [10]. The integration of the modified formula (1) results in:

$$2 \cdot m \cdot (v(t = t_f) - v(t = 0)) = L'_{eff} \int_{t=0}^{t=t_f} I^2 dt. \qquad (2)$$

Assuming an initial velocity of $v(t = 0) = 0$ m/s, this equation simplifies to:

$$2 \cdot m \cdot v = L'_{eff} \int_{t=0}^{t=t_f} I^2 dt. \qquad (3)$$

Here v is the end velocity of the projectile after the acceleration. This formula shows that the end velocity is proportional to the action integral ($\int I^2 dt$) and inversely proportional to the mass of the projectile. For a given set of data points, drawing the left hand side of equation (3) versus the action integral should result in a linear relation, with the slope being the effective inductance gradient, L'_{eff}. To verify this relation and to determine the value of the effective inductance gradient a series of 3-d COMSOL simulations was performed, using a normalized pulse shape closely resembling the experimental current pulse. Two parameters, the peak current and the mass of the projectile were varied. The current pulse was scaled to a peak amplitude ranging from 100 kA to 200 kA in steps of 20 kA, and for each amplitude the mass of the projectile was changed from 60 g to 92 g, 120 g and 150 g. This simulation neglects friction, but includes joule heating. Figure 5 shows the validity of equation (3) over the full simulated parameter space. The end velocities range from 43 m/s (100 kA) to 160 m/s (200 kA) for the 60 g projectile and from 18 m/s to 68 m/s for the 150 g projectile. In the figure, the data points representing the simulations with the four different masses are mostly overlapping and differ only for the two largest values of the action integral by about three percent. This deviation can be regarded as the remaining uncertainty in the simulation. By fitting the data points with a line, the value of the effective inductance gradient can be determined to be $L'_{eff} = 0.478 \pm 0.009\,\mu$H/m.

2.2. Comparison to Experimental Data

For a comparison of experiment and simulation, different variables can be looked at. Some obvious candidates are the position of the projectile and the acceleration or velocity as a function of time. Figure 6 shows such a direct comparison. Feeding the experiment and simulation with a current pulse, the projectile is accelerated and will reach, when the current has decayed, its end velocity. Using the above mentioned 3%

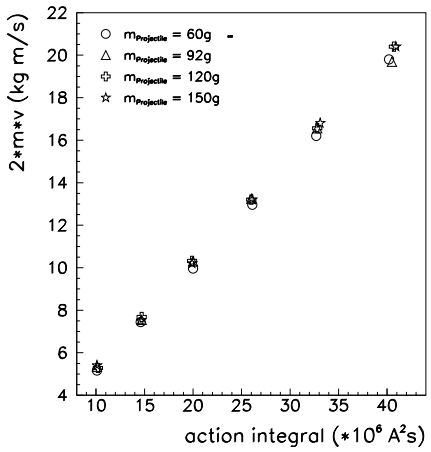

Fig. 5. The mass-scaled velocity of the projectile as a function of the action integral for four different projectile masses (COMSOL 3-d railgun simulation).

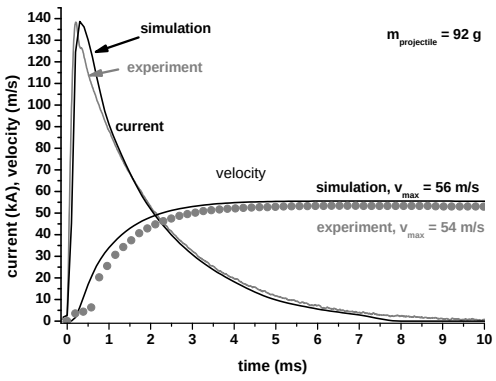

Fig. 6. Comparison between experimental and simulated data. Shown are the current distributions and the resulting velocity profiles for a projectile weight of 92 g.

as error estimate for the simulation and assuming that the error from the Doppler radar measurement above the above mentioned 0.7 ms can be neglected, the simulation results in a velocity of (57 ± 1.7) m/s, while the experimental value is 54 m/s. Taking into account the slightly different current pulses (the action integral of the simulation is about 2% higher) and the neglected friction in the simulation, both velocities are in good agreement. This direct comparison has the disadvantage, that one needs to know the exact output of the current pulse from the pulse forming network and the mass of the projectile. If instead the mass-scaled velocity versus the action integral is compared, the mass and the current profile do not need to be the same in experiment and simulation, as long as the geometry of the launcher is correctly modeled. Figure 7 shows the values of a series of 20 experimental shots with the small caliber railgun $SR\backslash$3-60 and the simulation results for a projectile mass of $m = 92$ g. This mass corresponds to the average mass of the projectiles used in the experiment. The figure shows good agreement between the experimental and the simulation values. It also reveals that the experiment has an overall shot

to shot variation for the same action integral value of less than 5%. Without doing an additional fit to the experimental data, the effective inductance gradient, $L'_{eff} = 0.48\ \mu$H/m, as extracted from the 3-d COMSOL simulation can be used for the experimental setup. Further inspection of figure 7 shows one shot with a too low velocity for it's action integral (marked by "Plasma"). Inspecting the muzzle voltage profile for this shot gives evidence that during the launch the metal to metal contact between the armature and the rails was lost and plasma developed. This plasma results in additional resistance and therefore more energy is lost that can not be used for acceleration. Turning this around, such an analysis can be used to identify shots with anomalies.

3. CONCLUSION

Using the COMSOL Multiphysics simulation program a dynamic 3-d simulation of the small caliber SR\3-60 railgun was implemented. This setup was used to calculate the effective inductance gradient to $L'_{eff} = 0.48\,\mu$H/m. Further on a series of experiments with the SR\3-60 was performed and compared to the simulation. This comparison included the velocity history of the shots and the mass scaled velocity versus the action integral. Overall good agreement between simulation and experiment was found. Thus it was shown that the simulation of the dynamics of railgun acceleration is possible. In the future it is planned to extend the simulation to higher velocities and more complicated setups. Improving the spatial resolution of the 3-d simulation, it should be possible to investigate the velocity skin effect and use this simulation to interpret magnetic field measurements taken with the sub-millimeter scale colossal magneto-resistance effect sensor [21] at railguns.

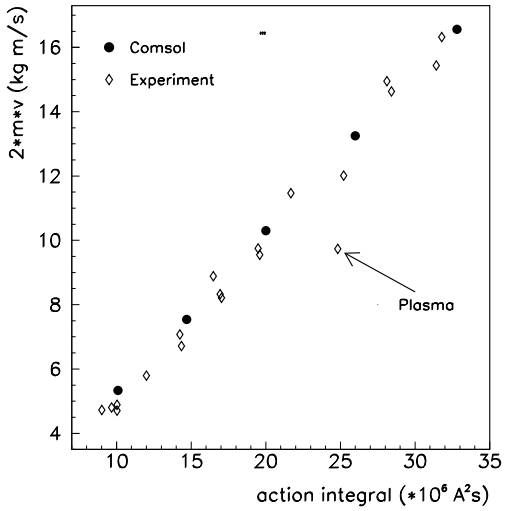

Fig. 7. The mass-scaled velocity of the projectile for simulations using COMSOL and 20 experimental railgun shots.

ACKNOWLEDGMENT

Part of this work was financed by the french ministry of defense (DGA) under the grant DGA/UM 05.55.405. The author acknowledges the work of J. Füllbier, who did setup the COMSOL simulation of a railgun in the context of his Master thesis at ISL. In addition the author would like to thank the members of the electromagnetic acceleration group, who contributed through discussions and the relentless efforts in the experimental hall to the success of this research.

REFERENCES

1. L. Abdelhamid, H. Amimeur and L. Bahmed, *Analysis and Simulation of the various Generators used in Wind Systems*, In: JEE Journal of Electrical Engineering, Vol. 10, 2010, Ed. 1, Art. 4, *http://www.jee.ro*.
2. N. Mohdeb and M. R. Mekideche, *A new simulated Annealing for solving Geometrical Shape Optimization of a Linear Actuator* In: JEE Journal of Electrical Engineering, Vol. 10, 2010, Ed. 2, Art. 24, *http://www.jee.ro*.
3. I. R. McNab and F. C. Beach, *Naval Railguns*, In: IEEE Transactions on Magnetics, Vol. 43, No. 1, January 2007.
4. I. R. McNab, *Progress on Hypervelocity Railgun Research for Launch to Space*, In: IEEE Transactions on Magnetics, Vol. 45, No. 1, January 2009.
5. H. Kolm, P. Mongeau, F. Williams, *Electromagnetic Launchers*, In: IEEE Transactions on Magnetics, Vol. 15, No. 5, September 1980.
6. M. W. Tompkins, M. A. Anderson, Q. Feng, J. Zhang, K. Kim, *Study of a Transaugmented Two-Stage Small Circular-Bore Railgun for Injection of Hypervelocity Hydrogen Pellets as a Fusion Reactor Refueling Mechanism*, In: IEEE Transactions on Magnetics, Vol. 33, No. 1, January 1997.
7. T. Siaenen, M. J. Löffler, *Comparison between Linear Electromagnetic Accelerators*, *Proceedings of the 2nd Euro-Asian Pulsed Power Conference*, Vilnius, Lithuania, September 22-26, 2008, In: Acta Physica Polonica A, Vol. 115 (2009), pp. 1089.
8. J. L. Upshaw, J. P. Kajs, *Micrometeoroid Impact Simulations using a Railgun Electromagnetic Accelerator*, In: IEEE Transactions on Magnetics, Vol. 27, No. 1, January 1991.
9. R. Marshall, W. Ying, *Railguns: Their Science and Technology*, Beijing, China, China Machine Press, 2004.
10. W. Ying, R. A. Marshall, C. Shukang, *Physics of Electric Launch*, Beijing, China, Science Press, 2004.
11. As. Keshtkar, T. Maleki, A. Kalantarnia, Ah. Keshthkar, *Determination of Optimum Rails Dimensions in Railgun by Lagrange's Equations*, In: IEEE Transactions on Magnetics, Vol.45, No.1, January 2009.
12. M. Crawford, R. Subramanian, T. Watt, D. Surls, D. Motes, J. Mallick, D. Barnette, S. Satapathy, J. Campos, *The Design and Testing of a Large-Caliber Railgun*, In: IEEE Transaction on Magnetics, Vol.45, No.1, January 2009.
13. G. A. Shvetsov, S. V. Stankevich, *Comparison Between 2-D and 3-D Electromagnetic Modeling of Railgun*, In: IEEE Transaction on Magnetics, Vol.45, No.1, January 2009.
14. *http://www.comsol.com*, Comsol Multiphysics Simulation (Version 3.5a).
15. S. Hundertmark,G. Vincent, *Performance of a hexagonal, segmented railgun*, Pulsed Power Conference, 2009 IET European, 21-25 Sept. 2009.
16. F. W. Grover, *Inductance Calculations: Working Formulas and Tables*, New York, USA, D. Van Nostrand Company, 1946.
17. H. Hertwig, *Induktivitäten*, Berlin, Germany, Verlag für Radio-Foto-Kinotechnik, 1954.
18. As. Keshtkar, S. Bayati and Ah. Keshtkar, *Derivation of a Formula for Inductance Gradient Using Intelligent Estimation Method*, In: IEEE Transactions on Magnetics, Vol. 45, No. 1, January 2009.
19. *Comsol Multiphysics, AC/DC Module*, AC/DC Model library, manual, Comsol AB, Stockholm, Sweden, October 2007.
20. J. Füllbier, *Modellierung eines Schienenbeschleunigers mit dem Simulationsprogramm COMSOL*, In: Master Thesis (in German), Fachhochschule Gelsenkirchen, May 2010.
21. O. Liebfried, M. Löffler, M. Schneider, S. Balevicius, V. Stankevic, N. Zurauskiene, A. Abrutis and V. Plausinaitiene, *B-Scalar Measurements by CMR-Based Sensors of Highly Inhomogeneous Transient Magnetic Fields*, In: IEEE Transaction on Magnetics, Vol. 45, No. 12, December 2009.